coatings

MDPI

Article

Long-Term Mechanical Deterioration Trends and Mechanisms of SBS-Modified Asphalt Mixtures

Jinquan Wang [1,2] and Maijian Liu [1,*]

[1] School of Transportation, Southeast University, Nanjing 211189, China; 18291903027@163.com
[2] Ningbo Hangzhou Bay Bridge Development Co., Ltd., Ningbo 315033, China
* Correspondence: 230219235@seu.edu.cn; Tel.: +86-139-2994-0398

Abstract: Understanding the long-term performance deterioration trends and mechanisms of asphalt pavement is crucial for effective maintenance strategies. This study characterizes and correlates the multi-scale performance deterioration of a 14-year asphalt pavement. Air void measurements, indirect tensile (IDT) fatigue testing, Fourier transform infrared spectroscopy (FTIR), and dynamic shear rheometer (DSR) testing were conducted on pavement cores and recovered binder. Multiple regression analysis was then performed on various performance indicators. Laboratory results indicate that the chemical composition and viscoelastic properties of SBS-modified binders evolve rapidly in the first few years, followed by a relatively stable aging rate. After 14 years, the mechanical and rheological properties of lower-layer mixtures deteriorate to a similar degree as the surface layer. Correlation analysis revealed that the residual strength of the mixture is more influenced by air voids, while reductions in fatigue life are primarily driven by binder aging. These findings highlight the necessity of applying preventive maintenance within the first 3–5 years to rejuvenate the surface asphalt and rehabilitate both the surface and underlying layers after long-term service.

Keywords: asphalt pavement; long-term deterioration; Fourier transform infrared spectroscopy (FTIR); fatigue life; dynamic shear rheology (DSR); multiple linear regression model

Citation: Wang, J.; Liu, M. Long-Term Mechanical Deterioration Trends and Mechanisms of SBS-Modified Asphalt Mixtures. *Coatings* **2024**, *14*, 1363. https://doi.org/10.3390/coatings14111363

Academic Editor: Valeria Vignali

Received: 26 September 2024
Revised: 21 October 2024
Accepted: 23 October 2024
Published: 26 October 2024

1. Introduction

Styrene-butadiene-styrene (SBS) modified asphalt is widely used in high-grade road and bridge pavements due to its superior performance and cost-effectiveness. However, due to an inadequate understanding of the deterioration mechanism in SBS-modified asphalt mixtures, highway agencies continue to face challenges in developing preventive maintenance strategies [1]. Untimely and inappropriate maintenance could significantly impair the operational efficiency and economic benefits of the road network. This knowledge gap highlights the urgent need to enhance our understanding of SBS-modified asphalt mixture deterioration to support effective maintenance strategies.

Over the past few decades, extensive research has been conducted on the field deterioration mechanisms of SBS-modified asphalt pavements, focusing on asphalt aging and the mechanical degradation of the mixture.

Regarding the aging of SBS-modified asphalt binder, numerous efforts have been undertaken to characterize the field aging behavior in terms of rheological properties, microstructure, and chemical composition. Zhang et al. [2] reported that the content of SBS polymer decreased to 20% after five years of service, with an aging gradient emerging during this period [3]. Zhang et al. [4] characterized the high-temperature performance grade (PG) of field-aged warm mix binder with service periods ranging from one to seven years, suggesting the use of softer binder to decelerate aging. Rasool et al. [5] characterized the aging depth of pavements after six and nine years of field aging, reporting that the top layer (1.2 cm) exhibits more severe aging. Ding et al. [6] investigated the field aging of asphalt across 14 highway sections, revealing a strong correlation between the carbonyl

index and environmental factors such as solar radiation and temperature. Wang [7] noted that, after two to three years of service, the high-temperature performance grade (PG) of the binder increased by 20 to 30%.

Regarding the mechanical performance evolution of SBS-modified asphalt mixtures, Luo reported the dynamic modulus of field cores in Texas increased by approximately 70% and 130% at the end of 8 and 14 months, respectively [8]. Cui et al. [9] suggest that the fatigue behavior of both the surface and underlying layers deteriorated to a similar extent after eight to ten years of field service. Gu et al. [10] found that the cracking resistance of field cores decreased significantly from the first to the ninth month, with a slower decline from the ninth to the fifteenth month. Additionally, to explore the influencing factors of asphalt pavement deterioration, Woo et al. [11] examined the effect of the connected void ratio on the depth of pavement aging. Wang et al. [7] suggest that asphalt aging does not linearly affect the pavement mixture modulus. Jing et al. [12] investigated the field evolution of asphalt aging and mixture stiffness in porous pavement, demonstrating that air-void distribution significantly influences aging sensitivity.

The impact factors, performance indicators, and pavement service years in the aforementioned studies are summarized in Table 1. Based on the analysis of Table 1, two research gaps were identified:

(1) Previous studies have primarily focused on the short- and mid-term performance deterioration of pavements (generally less than 10 years), hindering the establishment of long-term deterioration patterns.
(2) Although external factors such as service life and climate conditions have been extensively studied, the combined effects of internal factors, such as air voids and asphalt aging, on the mechanical deterioration of pavements are not yet fully understood.

Table 1. Summary of previous studies on asphalt pavement deterioration.

Impact Factors	Pavement Performance Indicators	Field Service Time	Ref
Service year	Binder rheological properties, chemical composition, and fluorescence morphology	1, 5 year	[2]
Service year, pavement depth		1, 5 year	[3]
Service year, pavement depth		6, 9 year	[5]
Service year, WMA technology, climate	Binder high-temperature PG	0~7 year	[4]
Service year		0, 2, 3 year	[7]
Binder type, air void content, pavement depth, temperature, aging time	Mixture dynamic modulus	1~14 months	[8]
Service year, pavement depth	Binder's rheological properties, chemical composition, and mixture dynamic modulus	0, 1, 2, 3 year	[13]
Failure types, traffic load, service time	Mixture residual fatigue properties	7, 8, 10 year	[9]
Service year, air void, WMA technology	Mixture fracture properties	1~15 months	[10]
Binder aging	Mixture rutting depth, dynamic modulus	0, 2, 3 year	[7]
Service year, air void	Binder rheological properties, chemical composition, mixture dynamic modulus	0~4 year	[12]

To address these gaps, this study examined and correlated the chemical, rheological, and mechanical properties of pavement cores with 0, 1, 5, and 14 years to enhance the understanding of asphalt pavement long-term deterioration.

2. Objective

The primary objective of this study was as follows:

(1) Examine the time-evolution trends of pavement air void, IDT strength, fatigue life, and binder's aging.
(2) Investigate the combined effect of air void and asphalt aging on mixture strength and fatigue deterioration.

The results of this study will help uncover the long-term evolution trends and mechanisms of pavement performance deterioration, facilitating early maintenance planning and the pre-allocation of funds. A flowchart of this study is shown below.

As illustrated in Figure 1, pavement cores with varying service years were collected. Air void measurements, indirect tensile (IDT) fatigue tests, Fourier transform infrared spectroscopy (FTIR), and dynamic shear rheometer (DSR) tests were conducted on core mixtures and recovered binders. Based on the test results, the time-evolution trends of pavement performance were derived. Additionally, FTIR and DSR results were correlated to investigate the impact of chemical composition variation on binder's viscoelasticity. Finally, multiple linear regression analyses were performed to examine the combined effects of air void content and aging on mixture mechanical deterioration.

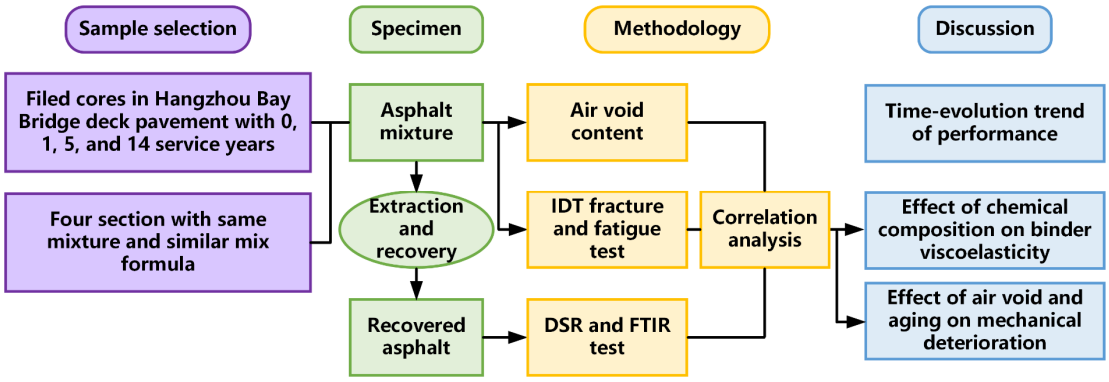

Figure 1. Flowchart of this study.

3. Methodology

This study characterizes the evolution of volumetric, chemical, rheological, and mechanical properties of core specimens taken from the Hangzhou Bay Bridge deck pavement across different service years. The multi-scale performance of the cored mixtures was first assessed using IDT, FTIR, and DSR tests. Based on these test results, the performance deterioration trend of the pavement over 14 years of service was characterized. Additionally, a mechanical degradation model for the pavement was established through multiple linear regression, considering the combined impacts of air voids and asphalt aging.

3.1. Project and Pavement Cores Information

The Hangzhou Bay Bridge, located in Zhejiang Province, China, connects the cities of Jiaxing and Ningbo. The bridge is exposed to a subtropical monsoon climate characterized by high humidity and significant rainfall, with the climate data summarized in Figure 2. The bridge has two layers of deck pavement: the upper layer consists of a 4 cm thick SMA 13 (Stone Mastic Asphalt with a nominal maximum aggregate size of 13 mm), and the lower layer consists of a 6 cm thick SMA 16 (Stone Mastic Asphalt with a nominal maximum aggregate size of 16 mm). The bridge was open to traffic in 2008 and the annual traffic volume data are presented in Figure 3. The Equivalent Single Axle Load (ESAL) is a standardized unit used to quantify the relative damage caused by various axle loads compared to a standard 100 kN single axle load.

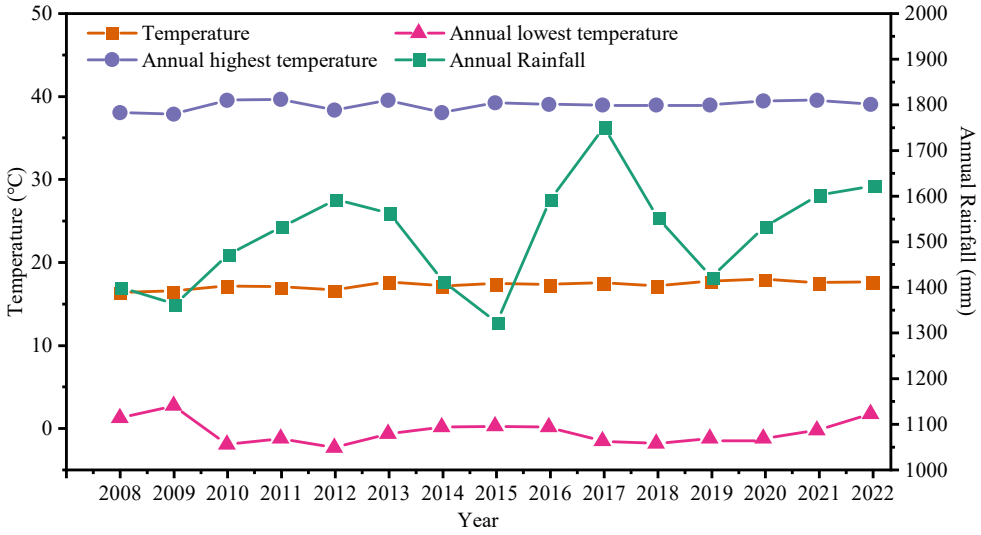

Figure 2. Annual climate data.

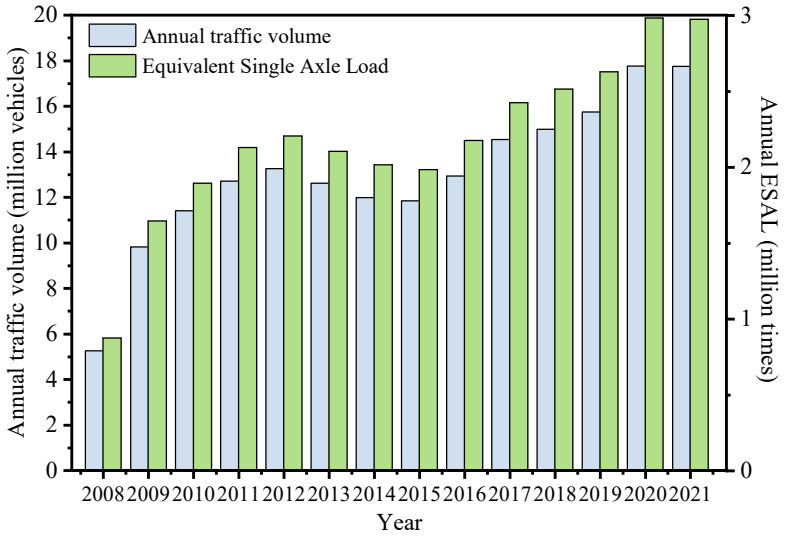

Figure 3. Annual traffic volume and ESAL.

During the bridge's service period, several sections of deck pavement were milled and repaved in 2017, 2021, and 2022 using same pavement structure and similar material compositions. In this study, core specimens were collected from both the repaved sections and sections that have not undergone repaving since the initial construction in 2008. All core specimens were drilled from the wheel path of the slow lane on the Hangzhou Bay Bridge in November 2021. Table 2 summarizes the detailed information of core samples. The full-depth cylindrical field cores have a diameter of 100 mm and a height of 100 mm. In the laboratory, the cores were separated into upper and lower layers and trimmed to a height of 40 mm, as depicted in Figure 4.

Table 2. Information of core samples.

Specimen Code	#0	#1	#5	#14
Service year	0	1	5	14
Paving time	2021.08	2020.02	2016.05	2008.03
Core collecting time	2021.11	2021.11	2021.12	2021.11
Millage for drilling	K1387 + 100–K1388 + 685	K1388 + 685–K1388 + 780	K1386 + 000–K1387 + 100	K1385 + 500–K1385 + 800
Height of cores (mm)	100	100	40 (upper layer)	100

Figure 4. Core samples of different service years.

The material properties and mix-design parameters of pavement cores are shown in Table 3 and Figure 5. As indicated in Table 3, core samples from different years utilized the same PG grade of SBS-modified asphalt, with mix design parameters and differing by no more than 5%.

Table 3. Material composition of different-year core specimens.

Service Years		0 Year		1 Year		5 Years	14 Years	
Binder property	Type	SBS-modified		SBS-modified		SBS-modified	SBS-modified	
	Penetration (0.1 mm)	56		58		53	50	
	Softening point (°C)	77		78		82	80	
	Ductility (5 °C, cm)	34		35		31	30	
	PG-grade	76–22		76–22		76–22	76–22	
Mixture property	Mixture type	SMA13	SMA16	SMA13	SMA16	SMA13	SMA13	SMA16
	Asphalt content (%)	5.8	5.5	5.6	5.7	5.7	5.7	5.6
	Fiber content	0.3	0.3	0.3	0.3	0.3	0.3	0.4
	VV	4.0	3.8	4.3	4.0	4.0	4.2	4.1
	VMA	17	17.9	17.8	17.5	17.5	16.65	16.8
	VFA	77.7	76.5	75.84	77.1	77.14	75.19	75.6
	Marshall stability	9.62	8.02	8.54	8.54	8.93	10.07	8.4

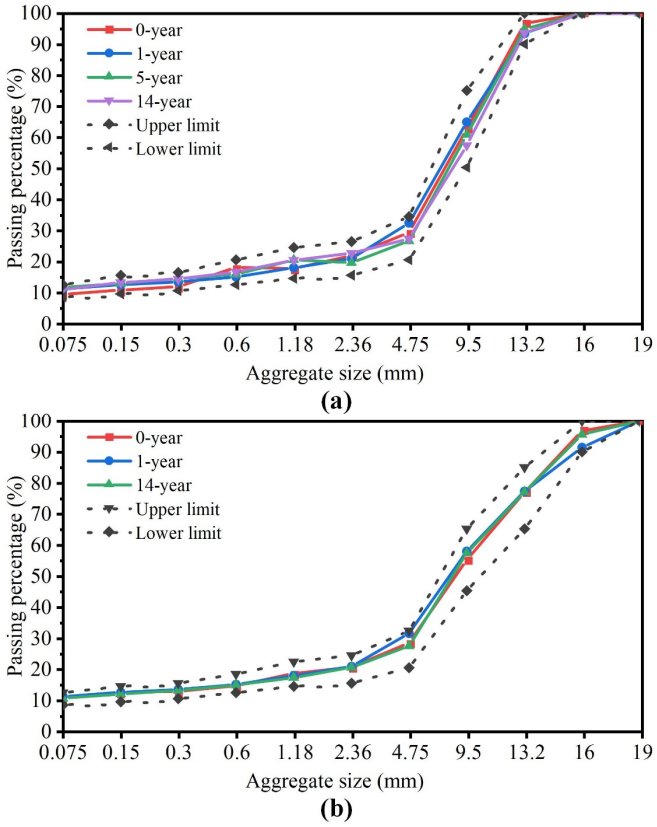

Figure 5. Gradation of pavement cores: (**a**) SMA 13 for upper layer, (**b**) SMA16 for lower layer.

3.2. Sample Preparation and Test Procedures

3.2.1. Sample Preparation

Pavement cores from various years were drilled from the pavement and measured for diameter and height. Subsequently, the air void ratio and indirect tension (IDT) tests were conducted on the mixture cores. After the IDT testing, the mixture cores were heated, dispersed, and then soaked in trichloroethylene to dissolve the asphalt binder. Finally, the field-aged binders were extracted and recovered according to AASHTO T 319 [14] and then underwent the FTIR and DSR test. A flowchart of sample preparation and performance test is summarized in Figure 6.

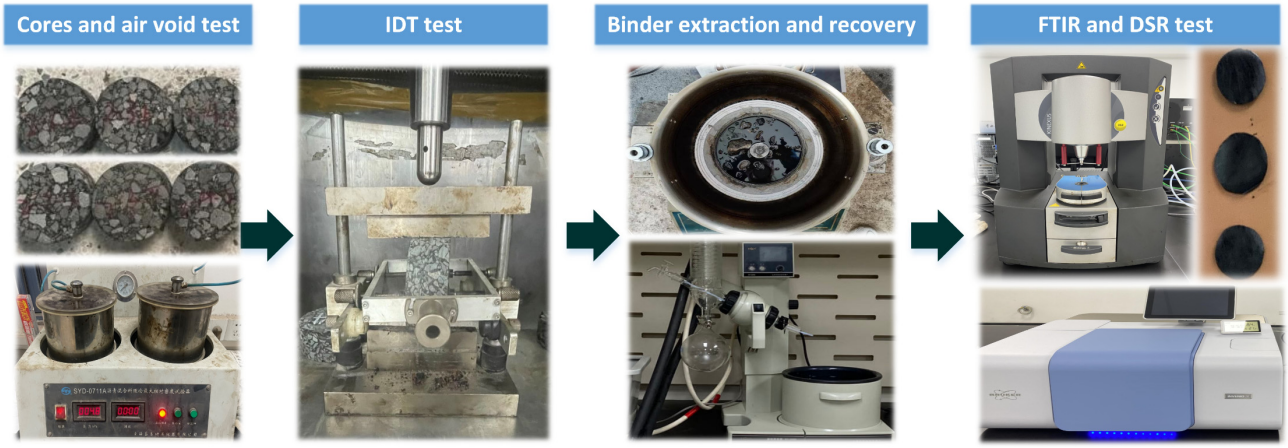

Figure 6. Flowchart of sample preparation and performance test.

3.2.2. Air Voids Content Testing

Bulk specific gravity and theoretical maximum specific gravity of the cored samples were first measured in accordance with AASHTO T166 [15] and AASHTO T209 [16]. Then, the total air void content (*TAV*) and accessible air void content (*AAV*), which refers to the air voids connected to the external environment, are calculated using the following equations:

$$TAV = (1 - \frac{G_{mb}}{G_m}) \times 100 \quad (1)$$

$$AAV = (\frac{m_s - m_a}{m_s - m_w}) \times 100 \quad (2)$$

where m_a = dry sample weight in air; m_s = saturated sample weight in air (surface dry); m_w = saturated sample weight in water; G_m = theoretical maximum specific gravity.

3.2.3. Fourier Transform Infrared Spectroscopy

The FTIR spectra of recovered binder with different service years were determined using a Bruker attenuated total reflection Fourier transform infrared (ATR-FTIR, INVENIO, Waltham, MA, USA.) spectrometer. The spectra were scanned with a wavenumber range of 400–4000 cm^{-1} and a resolution of 4 cm^{-1}. For each service year, three parallel samples were tested, and the results were averaged.

3.2.4. Dynamic Shear Rheometer (DSR) Test

The dynamic shear rheometer (DSR, Kinexus DSR, NETZSCH, Bavaria, Germany) test measures the viscoelastic properties of asphalt binders by applying oscillatory shear stress to a sample and recording its deformation response. In this study, the test mode of frequency sweep was applied to the recovered binder at frequencies ranging from 0.1 to 10 Hz and at temperatures of 25, 35, 45, 55, 65, and 75 °C. The strain was maintained at 1% to ensure rheological behavior within the linear viscoelastic range of all asphalt binders [17]. The complex modulus (G^*) and phase angle (δ) at various temperatures and frequencies were recorded, and rheological parameters such as the fatigue factor ($G^* \times \sin\delta$) and rutting factor ($G^*/\sin\delta$) were determined.

3.2.5. Indirect Tension (IDT) Fracture Test

The indirect tension (IDT) test characterizes the strength of asphalt mixtures by applying a load across the vertical diametral plane of a cylindrical specimen, which produces tensile stress in the lateral (horizontal) direction. In this study, the IDT fracture test was conducted in accordance with ASTM D6931 [18], at a temperature of 15 °C, employing a loading rate of 50 mm/min with the UTM-100 system (IPC Global, Melbourne, Victoria, Australia). The test was terminated upon reaching a load of less than 0.1 kN. Load-displacement curves were recorded and analyzed, as depicted in Figure 7. Subsequently, based on the load–displacement curve, the following parameters of interest were calculated by Equations (3) and (4) [19], adhering to ASTM D8225 [20].

(1) Indirect tensile strength S_T

$$S_T = \frac{2000 \times P_{100}}{\pi \times t \times D} \quad (3)$$

where P_{100} is the peak load (kN), t is the height of the specimen (mm), D is the diameter of the specimen (mm).

(2) Final displacement u (mm)
(3) Total fracture energy G_f

$$G_f = \frac{W_f}{D \times t} \quad (4)$$

where W_f represents the total fracture work, which corresponds to the area under the load-displacement curve.

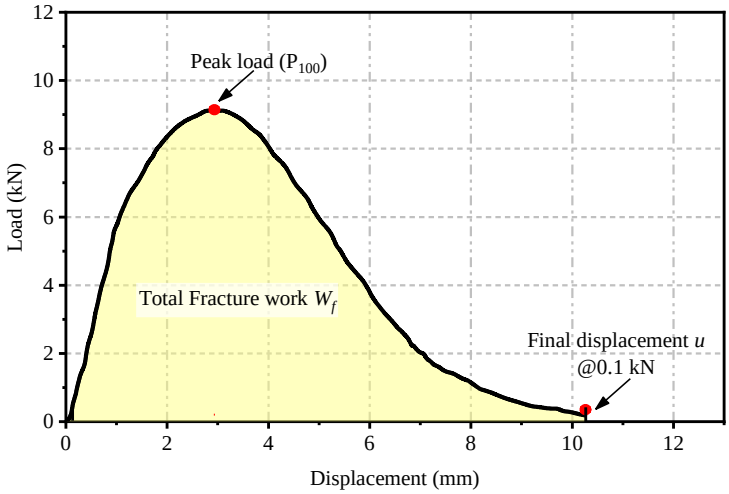

Figure 7. Load–displacement curve of IDT tests.

3.2.6. Indirect Tension (IDT) Fatigue Test

To assess the residual fatigue resistance of the SMA mixture, pavement cores were subjected to the indirect tension (IDT) fatigue test. The test was conducted at 15 °C in stress control mode, using a load frequency of 10 Hz and a haversine loading waveform, in accordance with AASHTO T-322 [21]. To determine the stress level for the IDT fatigue test, indirect tensile strength (ITS) tests were first conducted at 15 °C with a loading rate of 50 mm/min, in accordance with ASTM D6931 [18]. To ensure consistent stress levels, the indirect tensile strengths of samples with different service years were averaged. Then, the averaged tensile strength was multiplied by stress ratios of 0.2, 0.3, and 0.4 [22] to finally obtain the stress values applied in the IDT fatigue test.

4. Results and Discussion

4.1. Time-Evolution Trends of Performance

This section aims to characterize the long-term performance evolution trends of pavement to facilitate predictive and timely maintenance. The following section explores the time-dependent variations in air void content, asphalt chemical composition, and rheology, mixture strength, and fatigue life.

4.1.1. Air Void Content

As shown in Figure 8, the air void content of the pavement underwent a slight decrease after one year of service, indicating the post-compaction by the traffic load [23]. Similar results were also found in Wang's study [7], where the pavement void ratios decreased by 50% and 30% after two and three years of service, respectively. After the initial densification phase, internal micro-cracks gradually developed under repeated loading, resulting in an increase in TAV and AAV. After 14 years of service, TAV and AAV increased by 2.5 and 4 times, respectively. It is observed that the increasing rate of air void content accelerates over service years as the accumulated fatigue damage weakens pavement structural integrity, making it more susceptible to cracking. Additionally, the ratio of AAV to TAV gradually increased from 25% at 0 years to 35–45% at 14 years, attributed to the coalescence of existing accessible air voids with newly formed internal cracks [24]. Furthermore, the air voids in the upper and lower layers of the pavement exhibit similar trends in evolution, with the upper layer showing slightly higher air voids after 14 years of service.

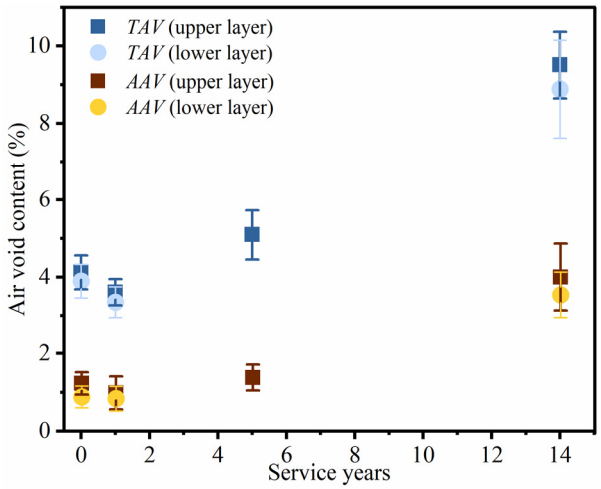

Figure 8. Air void content at different service years.

4.1.2. Binder's Chemical Compositions

The infrared spectra of recovered asphalt samples (which ranged from 600 to 3500 cm^{-1}) are shown in Figure 9. With prolonged service time, the absorption peak areas of carbonyl and sulfonyl groups continually increase due to asphalt oxidation. Simultaneously, the absorption peak intensity of butadiene gradually decreases due to the degradation of the polybutadiene chain segment in SBS polymer.

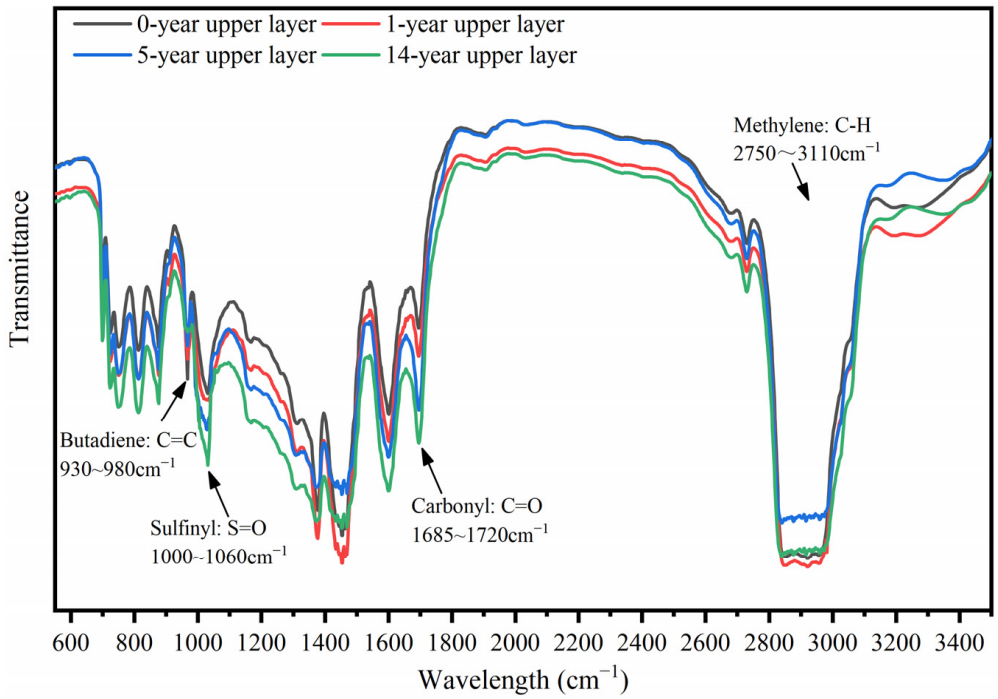

Figure 9. Local Fourier transform infrared spectra of recovered asphalt of different service years.

The chemical reactions during the aging of base asphalt and SBS polymer are illustrated in Figure 10. In base asphalt aging, oxygen initially reacts with perhydroaromatics to form hydroperoxides. These hydroperoxides subsequently decompose into radicals, which further react with oxygen to form ketones, resulting in the generation of carbonyl groups. In the case of SBS polymer, carbon-carbon double bonds decompose under heat to form free radicals, which then react with oxygen to form diketones.

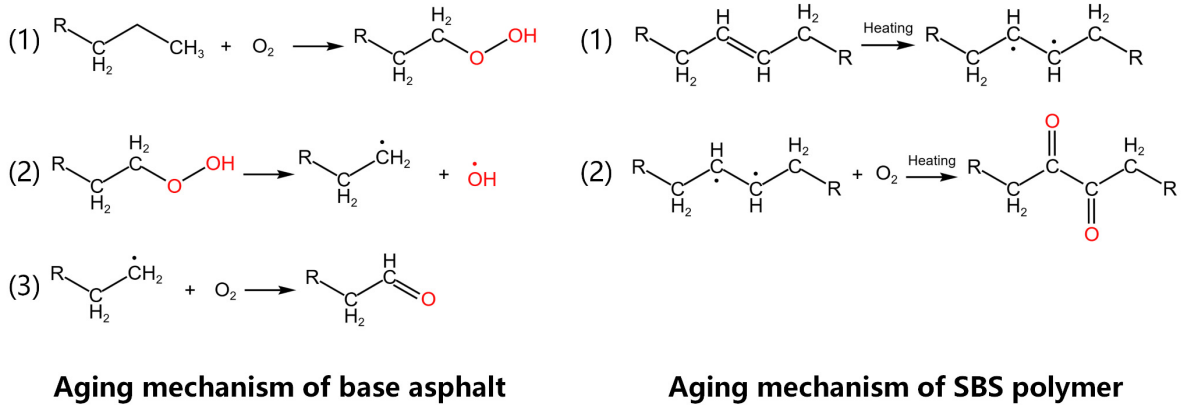

Figure 10. Aging reaction of base asphalt and SBS polymer.

To quantify the variation in functional group concentration after different years of aging, the absorption area of different characteristic peaks was first calculated using the linear baseline integral method. In this method, the integral baseline is determined by connecting the two points that mark the beginning and end of the peak. Then, the carbonyl index (*CI*), butadiene index (*BI*), and sulfoxide group index (*SI*) were calculated using the C-H peak as the reference [25], as shown in Equations (5)–(7).

$$CI = \frac{A_{C=O}}{A_{C-H}} \tag{5}$$

$$BI = \frac{A_{C=C}}{A_{C-H}} \tag{6}$$

$$SI = \frac{A_{S=O}}{A_{C-H}} \tag{7}$$

where $A_{C=O}$, $A_{C=C}$, $A_{S=O}$, $A_{C\text{-}H}$ is the absorption peak area of carbonyl, butadiene, sulfoxide group, and methylene groups. The integration intervals of these for absorption peak area are 1685~1720 cm^{-1}, 930~980 cm^{-1}, 1000~1060 cm^{-1}, and 2750~3110 cm^{-1}, respectively.

The evolution trend of the carbonyl index (*CI*), sulfoxide index (*SI*), and butadiene index (*BI*) is presented in Figure 11. Both the *CI* and *SI* exhibit a two-stage increase with extended service duration. Initially, these two indices rise rapidly, indicating a swift accumulation of oxidation products in the asphalt. Jing [13] also reported rapid aging in the first year, during which the carbonyl index doubled. As aging progresses, the rate of increase in both *CI* and *SI* decelerates, suggesting a gradual stabilization of the oxidation process. In contrast, the *BI*, which reflects the concentration of butadiene, shows a gradual decrease as SBS (styrene-butadiene-styrene) degrades over the service period.

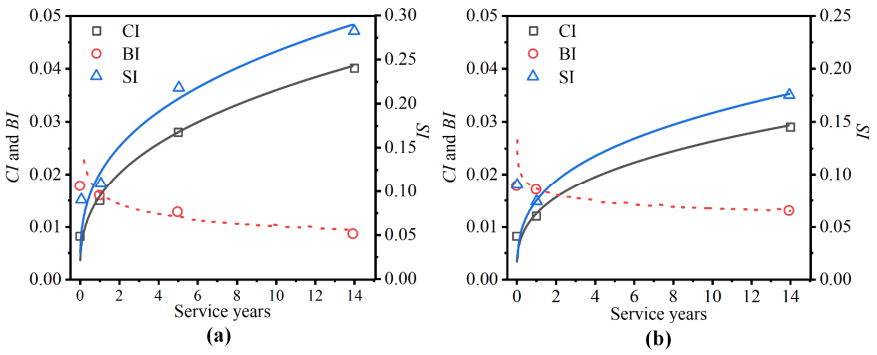

Figure 11. Infrared index at different service years: (**a**) upper-layer asphalt, (**b**) lower-layer asphalt.

Additionally, the lower layer exhibits a slower aging rate in initially service years. Zhang [3] also observed a 20–30% lower degree of aging in the underlying layer after 1.5 years of service. This slower aging rate in the lower layer can be attributed to reduced exposure to environmental factors such as UV radiation and oxygen. After 14 years, the *CI* and *SI* of the lower layer binder reach 80% of those observed in the upper layer. Similarly, the *BI* index of the lower layer is 50% higher than that of the upper layer, reflecting a smaller degree of SBS degradation in the lower asphalt.

4.1.3. Binder's Rheological Properties

The evolution trends of the complex modulus (G^*), phase angle (δ), fatigue factor ($G^* \times \sin\delta$), and rutting factor ($G^*/\sin\delta$) at 10 rad/s [17] are depicted in Figure 12. As shown in Figure 12a,b, the complex modulus at 25 °C and 65 °C exhibits a two-stage increase. In the first three years of service, the complex modulus nearly doubled, consistent with Zhang's findings [2]. After that the rate of increase slows, approaching a relatively constant rate of aging [4,8]. The initial rapid aging is attributed to the combined effects of oxidation and volatilization [8], whereas the subsequent slower aging process is primarily driven by oxidation. In the first five years, the upper-layer binder exhibits a complex modulus 20% higher than the lower layer, due to direct environmental exposure. This modulus gap is close to the results reported by Rasool [5]. As time progresses, the accessible air voids in the lower layer pavement rapidly develop, creating channels for oxygen and water penetration, thus accelerating the lower layer binder's aging. After 14 years of service, the modulus gap between the upper and lower layers is narrowed to less than 10%.

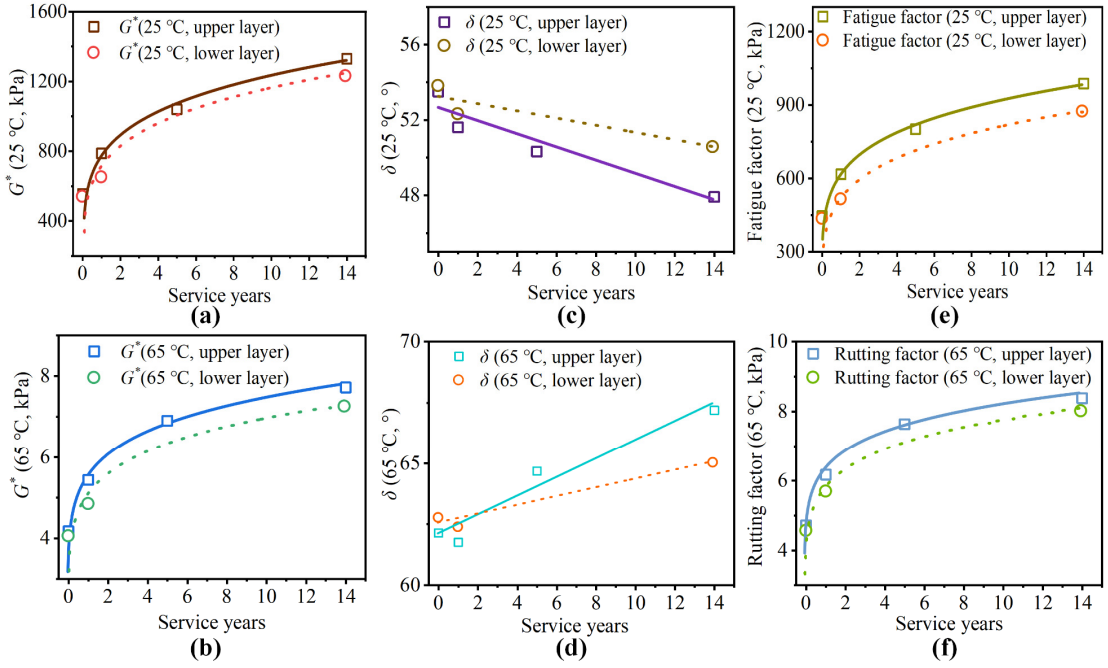

Figure 12. Binder's rheological property at different service years: (**a**) G^* at 25 °C, (**b**) G^* at 65 °C, (**c**) δ at 25 °C, (**d**) δ at 65 °C, (**e**) $G^* \times \sin\delta$, (**f**) $G^*/\sin\delta$.

As shown in Figure 12c,d, the phase angle at 25 °C gradually decreases with service life. This trend is due to the fact that at intermediate temperatures (25 °C), the viscoelastic properties of asphalt are primarily governed by the base asphalt. As the base asphalt hardens, the viscous component of the SBS-modified asphalt decreases, leading to a reduction in the phase angle. Conversely, at 65 °C, the phase angle exhibits a gradual increase. This is due to the fact that, at high temperatures (65 °C), the viscoelasticity of SBS-modified asphalt are more affected by the SBS polymer, as the viscosity of the base asphalt signifi-

cantly decreases. As aging progresses, degradation of the SBS polymer reduces the elastic component and increases the viscous component, thereby raising the phase angle at 65 °C.

Similarly, influenced by the complex modulus and phase angle, the rutting and fatigue factors also exhibit rapid growth in the initial years of service, followed by nearly stable growth in the later stages, as shown in Figure 12e,f. The increase in the rutting factor indicates an improvement in anti-rutting performance, while the rise in the fatigue factor suggests a decrease in fatigue resistance.

4.1.4. Indirect Tension (IDT) Strength

As observed in Figure 13, the IDT performance indicators of both upper and lower layer mixtures exhibit a similar decline trend. The deterioration rate for IDT strength and displacement basically remains stable, with a relatively fast decline in the first few years, consistent with the findings observed by Gu [10]. The lower layer mixture exhibits slight performance advantages over the upper layer in the first few years, but these advantages significantly shrink to about 10% after 14 years of service.

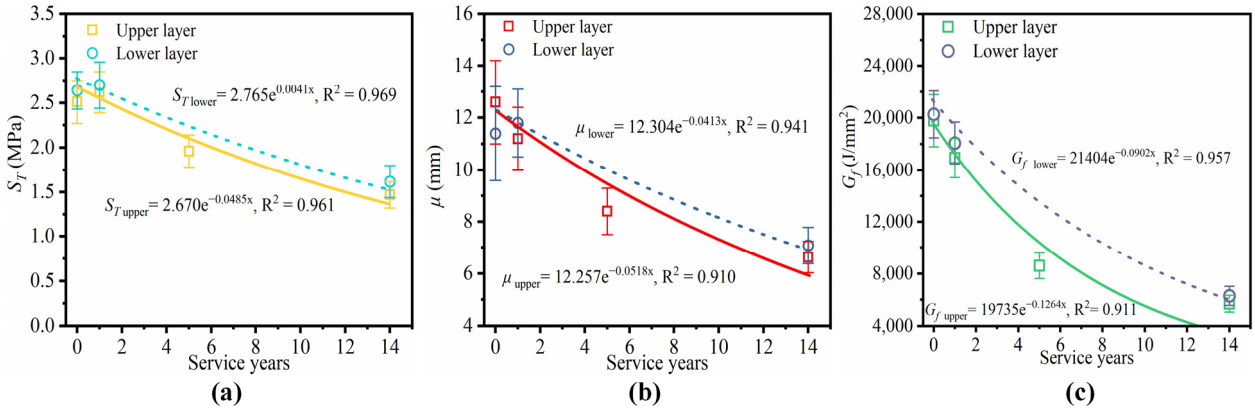

Figure 13. IDT test results at different service years: (**a**) IDT strength, (**b**) displacement, (**c**) fracture energy.

As depicted in Figure 13a, the strength of both the upper and lower layers is nearly identical after construction. After one year, the strength of both layers remains relatively stable, attributed to the densification and limited development of micro-cracks within the mixtures. After 14 years of service, the IDT strength of both layers decreases to about 55% of the initial strength due to accumulated fatigue damage and loss of binder adhesion.

Figure 13b shows that the upper and lower layer mixtures exhibit similar displacement at the start of service. However, after one year, the displacement of the upper layer significantly decreases due to the rapid aging of the surface binder. This rapid decline in flexibility observed in the first year is also noted in Gu's study [10]. After 14 years of service, the lower layer shows only 8% higher displacement than the upper layer, as its air void content and asphalt aging have developed to a level comparable to that of the upper layer.

As shown in Figure 13c, the fracture energy exhibits a similar downward trend, which can be inferred from the strength and displacement curves. After 14 years of service, the fracture energy of both layer mixtures declines to approximately one-fourth of their initial values, aligning with the findings observed in study [22].

4.1.5. Indirect Tension (IDT) Fatigue Life

To ensure a consistent stress level, the IDT strength for different service years was averaged to obtain a mean IDT strength value of 2.23 MPa. Stress ratios of 0.2, 0.3, and 0.4 were then applied to determine the three stress levels of 0.45 MPa, 0.65 MPa, and 0.90 MPa, referred to as S1, S2, and S3, respectively. Fatigue life in this section is defined as the total number of load cycles leading to complete fracture of the specimen [26]. The fatigue life for various service years is summarized in Figure 14.

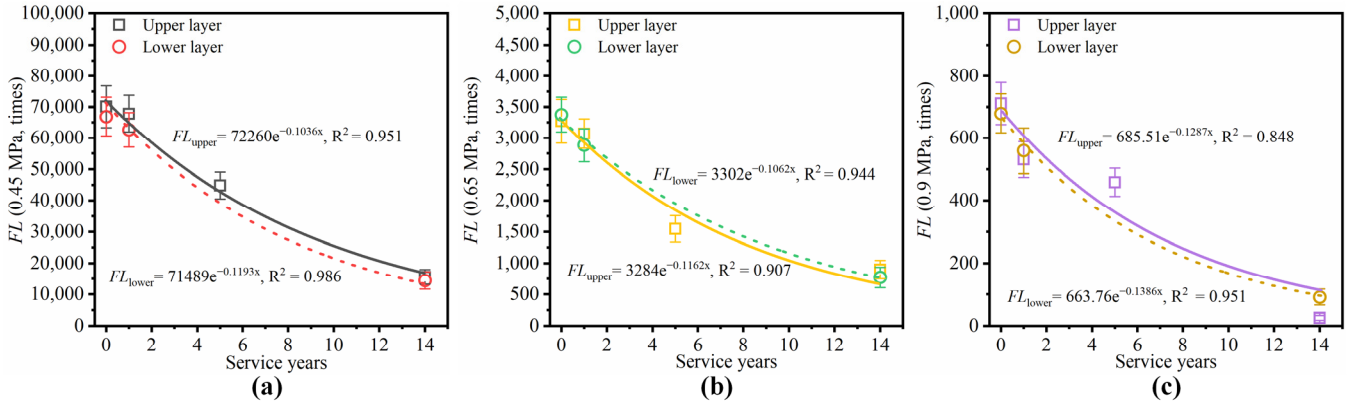

Figure 14. Fatigue life at different service years and stress levels: (**a**) 0.45 MPa, (**b**) 0.65 MPa, (**c**) 0.9 MPa.

As shown in Figure 14, the fatigue life exhibits a similar exponential decline to the IDT strength. The upper and lower layer mixtures exhibit generally similar values and evolution patterns of fatigue life [9]. The similar degree of fatigue degradation in the two pavement layers may be attributed to a higher level of aging while a lower tensile stress level in the upper layer [27]. After 14 years of service, the fatigue life of both layers decreased to 20% of its original value. The similar residual fatigue life of the surface and underlying layers after long-term service (8 to 10 years) was also noted by Cui [9].

Notably, as shown in Figure 14c, at a high stress ratio of 0.9 MPa, the upper layer mixture demonstrates a significantly lower fatigue life of only 25 cycles compared to the lower layer, indicating increased stress sensitivity.

To further characterize the fatigue performance, a fatigue model was fitted using Equation (8), and the fitted parameters are displayed in Table 4.

$$N_f = K\left(\frac{1}{\sigma_0}\right)^n \tag{8}$$

where N_f represents the fatigue cycles, σ_0 denotes the stress level, and K and n are the fitted parameters affected by materials' fatigue properties.

Table 4. Fitted parameter fatigue equation.

Layer	Service Year	K	*n*	R^2
upper	0	89.993	−8.382	0.999
lower		103.481	−8.129	0.999
upper	1	84.034	−8.454	0.999
lower		76.692	−8.383	0.999
upper	5	30.879	−9.135	0.999
upper	14	25.486	−7.933	0.999
lower		30.730	−7.816	0.999

In Table 4, the K value represents the level of fatigue life for asphalt pavement, and n indicates the attenuation rate of fatigue life under increasing stress levels, namely stress sensitivity. As shown in the table, the upper and lower layers have similar K values, which implies that they have comparable fatigue life. Additionally, the higher n value for the upper layer indicates its greater stress sensitivity, consistent with the observations in Figure 14.

4.2. Correlation of Binder's Chemical Composition and Rheology

To investigate the relationship between the chemical composition and rheological properties of field-aged SBS-modified asphalt. The correlation analysis was conducted on

chemical indicator (*CI* and *BI*) and rheological indicators (G^* and δ at 25 °C and 65 °C). The selected variables were first normalized to the deterioration ratio (*DR*) using Equation (9)

$$DR_{index} = \frac{Index\ value_{0,1,4,15\ years} - Index\ value_{0\ year}}{Index\ value_{0\ year}} \times 100\% \quad (9)$$

The scatter plot of chemical–rheological indicators is presented in Figure 15, and the results of the linear regression analysis are summarized in Table 5. To validate the sample size for linear regression, a post hoc power analysis was conducted using a *t*-test in G*Power software. The analysis yielded power values above 0.8 for all models, confirming a sufficient sample size to detect the expected effects with high confidence.

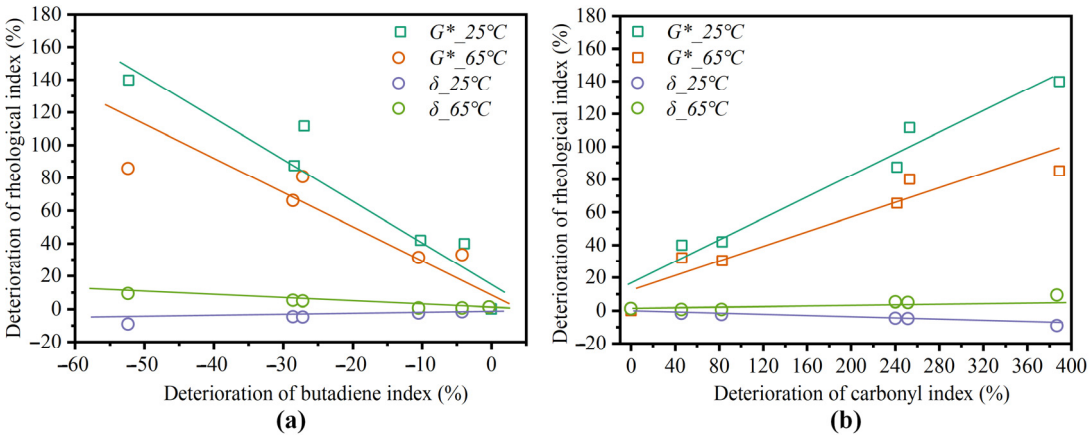

Figure 15. Binder chemical and rheological correlation results: (**a**) *CI* and rheological indicators, (**b**) *BI* and rheological indicators.

Table 5. Linear regression results of binder's chemical and rheological performance indicators.

Deterioration Ratio of Variables		Fitted Coefficients		R^2	*p*-Value
X	Y	Slope	Intercept		
CI	G^*_25 °C	0.353	8.834	0.956	8.656×10^{-5}
	G^*_65 °C	0.226	9.162	0.895	7.769×10^{-4}
	δ_25 °C	−0.024	−0.615	0.937	1.374×10^{-4}
	δ_65 °C	0.021	−0.962	0.879	7.171×10^{-4}
BI	G^*_25 °C	−2.675	13.485	0.900	6.925×10^{-4}
	G^*_65 °C	−1.678	12.667	0.805	0.0038
	δ_25 °C	0.187	−0.853	0.947	1.366×10^{-4}
	δ_65 °C	−0.165	−0.794	0.929	2.864×10^{-4}

In Table 5, a larger R^2 value indicates a stronger correlation, while a smaller *p*-value signifies greater sensitivity of the dependent variable to the independent variable. As observed in Table 5, there is a strong linear relationship between various chemical compositions and viscoelastic indices, indicated by R^2 values greater than 0.8 and *p*-values significantly smaller than 0.05. The carbonyl index (*CI*) shows a higher correlation with the complex modulus (G^*) compared to the phase angle, as evidenced by the higher R^2. The strong correlation between *CI* and modulus is further supported by their similar two-stage variation trends shown in Figures 11 and 12a. Conversely, the phase angle (δ) exhibits higher sensitivity to binder index (*BI*) compared to *CI*, especially at high temperatures, as indicated by the smaller *p*-value. This suggests that the viscoelastic behavior of modified asphalt is primarily affected by the SBS polymer.

4.3. Correlation of Air Void, Aging, and Mechanical Performance

It is generally accepted that the mechanical performance deterioration of asphalt pavement is primarily controlled by the evolution of air voids and binder's viscoelasticity. This section investigates combined effects of these two factors on pavement mechanical deterioration using multiple linear regression analysis. The performance indexes used for linear regression are summarized in Table 6. Similarly, the selected variables were first normalized to the deterioration ratio (*DR*) using Equation (9) before conducting the correlation analysis. Each performance model was fitted by 21 data points collected from the upper and lower-layer cores. To assess sample size adequacy for multiple regression, a post hoc power analysis using an F-test in G*Power was performed. All models achieved power values exceeding 0.8, indicating that the sample size was adequate for effectively detecting correlations between the variables.

Table 6. Selected performance indicators for mechanical correlation analysis.

Independent Variables		Dependent Variables
Air content indexes:	Total air voids (*TAV*) Accessible air voids (*AAV*)	IDT strength (S_T) Fracture energy (*FE*) IDT fatigue life at 0.45 MPa (*FL*)
Asphalt rheological indexes:	Rutting factor (*RF*) Fatigue factor (*FF*)	

4.3.1. Strength Deterioration Model

The multiple linear correlation results between IDT strength (S_T) and various air void and rheological indicators are summarized in the Table 7. As shown in the table, the different regression models exhibit an R^2 exceeding 0.90, indicating a very strong correlation among residual strength, air void content, and rheological properties. The fitting coefficients indicate that strength is negatively correlated with air voids, rutting, and fatigue factors.

Table 7. Results of IDT strength multiple linear regression.

Deterioration Ratio of Variables			R^2	Fitted Coefficient			t-Value		*p*-Value	
X_1	X_2	Y_1		X_1	X_2	Intercept	X_1	X_2	X_1	X_2
TAV	*FF*	S_T	0.940	−0.211	−0.148	−0.128	−5.69	−3.04	<0.001	0. 007
TAV	*RF*		0.950	−0.221	−0.210	0.791	−7.78	−3.81	<0.001	0.001
AAV	*FF*		0.921	−0.075	−0.228	2.208	−4.48	−5.07	<0.001	<0.001
AAV	*RF*		0.909	−0.085	−0.301	2.878	−5.02	−4.46	<0.001	<0.001

In correlation analysis, larger absolute values of the t-value and smaller *p*-values indicate a greater impact of the predictor on the dependent variable. It is evident that both air void content and rheological indicators exhibit *p*-values smaller than 0.01, indicating both two factors significantly affect the mixtures' strength deterioration. Furthermore, the pavement strength exhibits greater sensitivity to air void, as indicated by larger absolute t-values and smaller *p*-values compared to rheological indicators [28]. This suggests the importance of tracking pavement air-void changes to predict the strength evolution. Moreover, *TAV* demonstrates a stronger correlation with IDT strength than *AAV*, possibly because IDT strength is more related to all cracks and voids within the mixture. In contrast, *FF* and *RF* exhibit a similar degree of correlation with IDT strength.

4.3.2. Fracture Energy Deterioration Model

Similarly, the evolution of fracture energy was correlated with air voids and the viscoelastic properties of the binder. As shown in Table 8, different regression models of fracture energy exhibit an R^2 exceeding 0.90, indicating a good a good fitting degree.

Like the strength model, different air void and rheological indicators all show a strong correlation to fracture energy, as indicated by *p*-values less than 0.01. Compared to air void, binder rheological indicators exhibit a greater impact on fracture energy, as indicated by the larger absolute value of the fitted coefficient and t-value. The significant influence of binder aging can be attributed to its hardening effect, which reduces the mixture's flexibility and maximum displacement, as illustrated in Figure 13b, thereby decreasing the fracture energy.

Table 8. Results of IDT fracture energy multiple linear regression.

Deterioration Ratio of Variables			R^2	Fitted Coefficient			t-Value		*p*-Value	
X_1	X_2	Y_1		X_1	X_2	Intercept	X_1	X_2	X_1	X_2
TAV	*FF*	*FE*	0.920	−0.196	−0.349	−0.008	−0.32	−4.30	0.005	<0.001
TAV	*RF*		0.932	−0.235	−0.464	1.361	−4.90	−4.97	<0.001	<0.001
AAV	*FF*		0.911	−0.069	−0.426	2.187	−2.72	−6.18	0.014	<0.001
AAV	*RF*		0.901	−0.084	−0.577	3.827	−3.33	−5.69	0.004	<0.001

4.3.3. Fatigue Life Deterioration Model

The correlation results of fatigue life (*FL*), air voids, and rheological properties are presented in Table 9. As shown in Table 9, different air void ratios (*TAV* and *AAV*) and rheological properties (*FF* and *RF*) all exhibit a strong negative linear relationship with fatigue life, as evidenced by the negative correlation coefficients. The rheological indices demonstrated larger absolute fitted coefficients and t-values compared to air void indicators, suggesting their greater influence on residual fatigue performance. This observation is also supported by the study of Sreedhar [29].

Table 9. Results of fatigue life multiple linear regression.

Deterioration Ratio of Variables			R^2	Fitted Coefficient			t-Value		*p*-Value	
X_1	X_2	Y_1		X_1	X_2	Intercept	X_1	X_2	X_1	X_2
TAV	*FF*	*FL*	0.982	−0.306	−0.351	0.245	−8.03	−9.19	<0.001	<0.001
TAV	*RF*		0.983	−0.345	−0.459	1.445	−8.38	−10.24	<0.001	<0.001
AAV	*FF*		0.977	−0.117	−0.447	2.173	−7.982	−11.210	<0.001	<0.001
AAV	*RF*		0.960	−0.134	−0.595	3.497	−7.311	−8.011	<0.001	<0.001

Based on the above analysis, the correlation models for strength, fracture energy, and fatigue life have demonstrated satisfactory R^2 values. Additionally, the normality of the model residuals has been confirmed, further validating the reliability of the regression model. Therefore, the regression model established in this study can potentially be used for predicting the residual performance of asphalt mixtures.

4.4. Insights and Significance for Future Pavement Maintenance

4.4.1. Insights for Pavement Maintenance

Based on the analysis of performance degradation trends and key impact factors discussed in this paper, the following insights are provided for future asphalt pavement maintenance:

(1) In common practice, maintenance is usually implemented when surface performance indicators, such as the Pavement Condition Index (PCI), reach a certain threshold. However, the surface-distress-based decision methods for pavement maintenance may not adequately capture the rapid aging observed in the first three years of service, as surface distresses may not yet be evident. Therefore, it is recommended to apply preventive maintenance, such as applying a fog seal after 3–5 years, to timely

rejuvenate aged asphalt surfaces. Additionally, aging degree assessments should be incorporated during early pavement inspections.

(2) In corrective maintenance and rehabilitation, pavement engineers typically need to conduct full-depth sampling of the asphalt layer to determine the treating depth. For the concrete bridge deck pavement discussed in this study, the surface and lower layers deteriorate to a similar degree after more than ten years of service. Therefore, when significant distresses are observed in the surface layer after long-term service, it can be inferred that the underlying layer has experienced similar deterioration, warranting the rehabilitation of both layers. This approach could eliminate the need for coring and testing of the lower layer pavement.

(3) In pavement inspections and sampling, the highway agency can predict pavement residual fatigue life using the performance prediction model proposed in Table 9. The predicted residual fatigue life provides a clear indication of the urgency for maintenance in specific road sections, facilitating early scheduling and budget allocation of maintenance.

Based on the aforementioned insights for maintenance, this study proposes a corresponding predictive maintenance plan and compares it with conventional maintenance plans based on pavement surface condition thresholds [30]. For the predictive maintenance plan proposed in this paper as shown in Table 10, the service life of the maintenance measures is set at the upper limit recommended by Chinese maintenance standards [31], as timely maintenance can prevent rapid pavement deterioration compared to addressing visible distress after it occurs. Accordingly, for conventional maintenance plans as shown in Table 11, the lifespan of the maintenance measures is set at the lower limit. In Tables 10 and 11, the full-depth rehabilitation signifies the end of the pavement life cycle.

Table 10. Predictive maintenance plan.

Application Year	Maintenance Measures	Life of Maintenance Measures (Year)	Note
3rd	Fog seal	3	Knowing aging trend of pavement
6th	Micro-surfacing	4	/
10th	Ultra-thin overlay (1.5 cm)	5	/
15th	Rehabilitation (End of pavement life cycle)	/	Knowing upper and lower layers deteriorate to same level

Table 11. Conventional maintenance plan.

Application Year	Maintenance Measures	Life of Maintenance Measures (Year)	Note
5th	Micro-surfacing	2	Based on the PCI threshold
7th	Ultra-thin overlay (1.5 cm)	4	/
11th	Mill and overlay (4 cm top surface)	4	Solely based on observed distress in the surface layer
15th	Rehabilitation (End of pavement life cycle)	/	/

4.4.2. Economic and Environmental Benefits

Based on the maintenance plans in Tables 10 and 11, a 1 km single-lane road segment is used as the analysis unit to determine the corresponding lifecycle maintenance costs and carbon emissions.

The costs and carbon emissions of different maintenance measures are first calculated as shown in Table 12, using the quota method. The costs and emission inventory data were collected from the Chinese quota specifications JTG/T3832-2018 [32], JTG/T3833-2018 [33], and the Inventory of Carbon & Energy (ICE) Version 2.0 [34]. Then, by summing the costs and emissions of individual maintenance activities over the service life, the lifecycle maintenance cost and carbon emission are obtained as shown in Table 13. As shown in the Table 13, the life cycle maintenance cost and carbon emissions are only 40% and 43% of those of the conventional maintenance plan. This highlights the lifecycle benefit of understanding performance evolution trends and conducting timely preventive maintenance.

Table 12. Costs and emissions of various maintenance activities per kilometer of lane.

Maintenance Activity	Cost ($)	Carbon Emission (t CO_2)
Fog seal	2255	0.803
Micro-surfacing	8782	6.158
Ultra-thin overlay (1.5 cm)	11,818	8.516
Mill and overlay (4 cm top surface)	34,964	20.432

Table 13. Lifecycle cost and carbon emissions for maintaining 1 km of a single lane.

Cost and Emission	Predictive Maintenance Plan	Conventional Maintenance Plan
Cost ($)	22,855	55,564
Carbon emission (t CO_2)	15.477	35.106

5. Conclusions

In this research, the mechanical performance of pavement cores with varying service years was characterized and correlated to investigate the long-term deterioration trend and mechanism of asphalt pavement. The main conclusions are summarized below:

1. The viscoelasticity of SBS-modified binder exhibits rapid and nonlinear deterioration during the first three years of service, followed by a relatively constant rate of aging. Accordingly, it is recommended to apply preventive maintenance, such as fog seals, within the first 3–5 years to rejuvenate the surface asphalt.
2. After 14 years, the air void and mechanical performance of lower-layer mixtures deteriorate to a similar degree as the surface layer. This suggests that, after a long-term service period, once significant distress is detected in the surface layer, it is recommended to repave both the upper and lower layers.
3. The complex modulus of SBS-modified asphalt exhibits stronger correlation with the carbonyl index (CI), indicating the base asphalt oxidation plays a major role in the binder's hardening. Conversely, the phase angle shows a higher sensitivity to the butadiene index (BI), suggesting that the viscous behavior of the binder is primarily affected by SBS polymer degradation, especially at high temperatures.
4. Both air voids and binder aging exhibit a significant impact on pavement mechanical deterioration, highlighting the necessity of adopting a lower air void ratio and incorporating anti-aging additives. Specifically, strength shows greater sensitivity to changes in air voids, while fatigue life demonstrates a higher dependency on the binder's viscoelastic properties.
5. The pavement mechanical deterioration can be effectively predicted by total air void (*TAV*), rutting factor (*RF*), and fatigue factor (*FF*), with R^2 values greater than 0.96.

The results presented herein can inform future pavement performance predictions and proactive maintenance strategies, thereby contributing to long-lasting and sustainable pavement. However, due to the limited data in this study, the asphalt pavement deterioration pattern was characterized only at the project level. Future work should incorporate

observations from other projects to develop more universal models for predicting pavement performance deterioration.

Author Contributions: Conceptualization, J.W.; methodology, M.L.; investigation, J.W. and M.L.; resources, J.W.; writing—original draft preparation, M.L. and J.W.; visualization, M.L.; supervision, J.W.; project administration, J.W.; funding acquisition, J.W. All authors have read and agreed to the published version of the manuscript.

Funding: This work was funded by the Transportation Science and Technology Project of Ningbo city (Funding Number: 202212).

Institutional Review Board Statement: Not applicable.

Informed Consent Statement: Not applicable.

Data Availability Statement: The data are contained within this article.

Conflicts of Interest: Jinquan Wang was employed by the Ningbo Hangzhou Bay Bridge Development Co., Ltd. The remaining authors declare that the research was conducted in the absence of any commercial or financial relationships that could be construed as a potential conflict of interest.

References

1. Wu, C.; Zhang, B.; Liu, J.; Si, W. Evolution Analysis of Asphalt Pavement Performance in Its Life Cycle: Case Study in Qinghai–Tibet Highway. *Sustainability* **2023**, *15*, 9600. [CrossRef]
2. Zhang, D.; Zheng, Y.; Yuan, G.; Guo, H.; Zhou, Q.; Qian, G.; Liang, B. Comparative Analysis of Rheological and Microscopic Performance of SBS Modified Asphalt Based on Field Aging and Laboratory Aging. *Fuel* **2023**, *352*, 128933. [CrossRef]
3. Zhang, D.; Zheng, Y.; Yuan, G.; Zhang, Y.; Qian, G.; Zhang, H. Research on the Field Aging Gradient Behavior of SBS-Modified Bitumen at Different Depths of Pavement by Rheological and Microscopic Characterization. *Fuel* **2022**, *329*, 125192. [CrossRef]
4. Zhang, W.; Shen, S.; Wu, S.; Mohammad, L.N. Long-Term Field Aging of Warm-Mix and Hot-Mix Asphalt Binders. *Transp. Res. Rec.* **2017**, *2632*, 140–149. [CrossRef]
5. tur Rasool, R.; Hongru, Y.; Hassan, A.; Wang, S.; Zhang, H. In-Field Aging Process of High Content SBS Modified Asphalt in Porous Pavement. *Polym. Degrad. Stab.* **2018**, *155*, 220–229. [CrossRef]
6. Ding, J.; Jiang, J.; Han, Y.; Ni, F.; Ma, X.; Chen, S. Chemical and Rheological Characterisation of In-Situ SBS Modified Asphalt Pavement Considering the Effect of Aging Gradient. *Int. J. Pavement Eng.* **2023**, *24*, 2099856. [CrossRef]
7. Wang, H.; Zhu, Y.; Zhang, W.; Shen, S.; Wu, S.; Mohammad, L.N.; She, X. Effects of Field Aging on Material Properties and Rutting Performance of Asphalt Pavement. *Materials* **2022**, *16*, 225. [CrossRef]
8. Luo, X.; Gu, F.; Lytton, R.L. Prediction of Field Aging Gradient in Asphalt Pavements. *Transp. Res. Rec.* **2015**, *2507*, 19–28. [CrossRef]
9. Cui, P.; Xiao, Y.; Fang, M.; Chen, Z.; Yi, M.; Li, M. Residual Fatigue Properties of Asphalt Pavement after Long-Term Field Service. *Materials* **2018**, *11*, 892. [CrossRef]
10. Gu, F.; Luo, X.; Zhang, Y.; Lytton, R.L. Using Overlay Test to Evaluate Fracture Properties of Field-Aged Asphalt Concrete. *Constr. Build. Mater.* **2015**, *101*, 1059–1068. [CrossRef]
11. Woo, W.J.; Chowdhury, A.; Glover, C.J. Field Aging of Unmodified Asphalt Binder in Three Texas Long-Term Performance Pavements. *Transp. Res. Rec.* **2008**, *2051*, 15–22. [CrossRef]
12. Jing, R.; Varveri, A.; Liu, X.; Scarpas, A.; Erkens, S. Differences in the Ageing Behavior of Asphalt Pavements with Porous and Stone Mastic Asphalt Mixtures. *Transp. Res. Rec.* **2021**, *2675*, 1138–1149. [CrossRef]
13. Jing, R.; Varveri, A.; Liu, X.; Scarpas, A.; Erkens, S. Laboratory and Field Aging Effect on Bitumen Chemistry and Rheology in Porous Asphalt Mixture. *Transp. Res. Rec. J. Transp. Res. Board* **2019**, *2673*, 365–374. [CrossRef]
14. *AASHTO T319*; Standard Method of Test for Quantitative Extraction and Recovery of Asphalt Binder from Asphalt Mixtures. AASHTO: Washington, DC, USA, 2022.
15. *AASHTO T166*; Standard Method of Test for Bulk Specific Gravity of Compacted Asphalt Mixtures Using Saturated Surface-Dry Specimens. AASHTO: Washington, DC, USA, 2013.
16. *AASHTO T209*; Standard Method of Test for Theoretical Maximum Specific Gravity and Density of Hot Mix Asphalt (HMA). AASHTO: Washington, DC, USA, 2013.
17. Zhang, H.; Chen, Z.; Xu, G.; Shi, C. Evaluation of Aging Behaviors of Asphalt Binders through Different Rheological Indices. *Fuel* **2018**, *221*, 78–88. [CrossRef]
18. *ASTM D6931*; Standard Test Method for Indirect Tensile (IDT) Strength of Asphalt Mixtures. ASTM: West Conshohocken, PA, USA, 2017.
19. Sun, J.; Luo, S.; Wang, Y.; Dong, Q.; Zhang, Z. Pre-Treatment of Steel Slag and Its Applicability in Asphalt Mixtures for Sustainable Pavements. *Chem. Eng. J.* **2023**, *476*, 146802. [CrossRef]

20. *ASTM D8225-19*; ASTM Standard Test Method for Determination of Cracking Tolerance Index of Asphalt Mixture Using the Indirect Tensile Cracking Test at Intermediate Temperature. ASTM: West Conshohocken, PA, USA, 2019.
21. *AASHTO T322*; Standard Method of Test for Determining the Creep Compliance and Strength of Hot-Mix Asphalt (HMA) Using the Indirect Tensile Test Device. Standard Test Method. AASHTO: Washington, DC, USA, 2011.
22. Wu, S.; Zhao, Z.; Xiao, Y.; Yi, M.; Chen, Z.; Li, M. Evaluation of Mechanical Properties and Aging Index of 10-Year Field Aged Asphalt Materials. *Constr. Build. Mater.* **2017**, *155*, 1158–1167. [CrossRef]
23. Hu, J.; Huang, Q.; Lou, N.; Luo, S. Microstructural Characteristics of Interfacial Zone in Asphalt Mixture Considering the Influence of Aggregates Properties. *Materials* **2020**, *13*, 2558. [CrossRef]
24. Shan, L.; Yang, H.; Guo, F.; Li, Z. Fatigue Damage Evolution in Asphalt Mixture Based on X-Ray CT Images. *Constr. Build. Mater.* **2022**, *358*, 129242. [CrossRef]
25. Sun, J.; Huang, W.; Lu, G.; Luo, S.; Li, Y. Investigation of the Performance and Micro-Evolution Mechanism of Low-Content Thermosetting Epoxy Asphalt Binder towards Sustainable Highway and Bridge Decks Paving. *J. Clean. Prod.* **2023**, *384*, 135588. [CrossRef]
26. Cao, W.; Mohammad, L.N.; Barghabany, P.; Cooper, S.B. Relationship between Laboratory and Full-Scale Fatigue Performance of Asphalt Mixtures Containing Recycled Materials. *Mater. Struct.* **2019**, *52*, 26. [CrossRef]
27. Pokorski, P.; Radziszewski, P.; Sarnowski, M. Fatigue Life of Asphalt Pavements on Bridge Decks. *Procedia Eng.* **2016**, *153*, 556–562. [CrossRef]
28. Zaltuom, A.M. A Review Study of the Effect of Air Voids on Asphalt Pavement Life. In Proceedings of the First Conference for Engineering Sciences and Technology, Giza, Egypt, 30 November 2018; Volume 2, pp. 618–625.
29. Sreedhar, S.; Coleri, E. Effects of Binder Content, Density, Gradation, and Polymer Modification on Cracking and Rutting Resistance of Asphalt Mixtures Used in Oregon. *J. Mater. Civ. Eng.* **2018**, *30*, 04018298. [CrossRef]
30. Rafiq, W.; Musarat, M.A.; Altaf, M.; Napiah, M.; Sutanto, M.H.; Alaloul, W.S.; Javed, M.F.; Mosavi, A. Life Cycle Cost Analysis Comparison of Hot Mix Asphalt and Reclaimed Asphalt Pavement: A Case Study. *Sustainability* **2021**, *13*, 4411. [CrossRef]
31. *JTG 5421-2018*; Specifications for Maintenance Design of Highway Asphalt Pavement. Ministry of Transport of the People's Republic of China: Beijing, China, 2019.
32. *JTG/T 3832-2018*; Budget Quota for Highway Works. Ministry of Transport of the People's Republic of China: Beijing, China, 2018.
33. *JTG/T 3833-2018*; Unit Prize of Highway Construction Machinery. Ministry of Transport of the People's Republic of China: Beijing, China, 2018.
34. Hammond, G.; Jones, C. *Inventory of Carbon & Energy (ICE)*; University of Bath: Bath, UK, 2008.